Spectral Profiling by 1D and 2D Electron Spin Resonance Imaging: Nitroxide Radicals in UV and Thermal Degradation of Poly(acrylonitrile−butadiene−styrene) Containing a Hindered Amine Stabilizer

Mikhail V. Motyakin and Shulamith Schlick*

Department of Chemistry, University of Detroit Mercy, Detroit, Michigan 48219-0900

Received October 3, 2000; Revised Manuscript Received February 5, 2001

ABSTRACT: Thermal and UV oxidative degradation of poly(acrylonitrile−butadiene−styrene) (ABS) containing a hindered amine stabilizer (HAS) was studied by electron spin resonance (ESR) spectroscopy and ESR imaging (ESRI). The imaging technique allowed digital (*nondestructive*) spectral profiling of the HAS-derived nitroxide radicals: Their intensity profile was determined by 1D ESRI, and the spatial variation of the ESR line shapes was determined by 2D spectral−spatial ESRI. The UV light was provided by fluorescent lamps with maximum intensity in the range 290−320 nm (UVB) or by a Xe arc that closely resembled the solar spectrum. Upon UVB irradiation the nitroxide signal was initially strong only on the irradiated side and increased with time through the sample. These results were taken as evidence for extensive damage on the irradiated side and slower thermal degradation in the entire sample. The effect of UVB radiation was in marked contrast with that of a Xe source; after Xe irradiation the nitroxide radicals were detected at both the irradiated side and the opposite side, and their intensity was negligible in the sample interior. Spatial variation of the ESR line shapes was observed for irradiation with both UV sources. The spatial distribution of the nitroxide radicals was, however, homogeneous during thermal degradation at 318 and 333 K, and there was no spatial variation of the ESR line shapes. The results allowed mapping of the line shape and intensity of nitroxide radicals within the sample as a function of treatment time and provided mechanistic details on the early stages of the degradation process. This study suggested a hierarchical variation of the HAS-derived nitroxide concentration: within morphological domains in ABS on the scale of a few micrometers and within the sample depth on the scale of millimeters.

Introduction

Exposure of polymeric materials to environmental conditions such as heat, mechanical stress, and ionizing or UV radiation in the presence of oxygen results in the formation of reactive intermediates that lead to degradation.[1−4] The degradation chemistry is complicated because even small amounts of chromophores, free radicals, and metallic residues from polymerization reactions can introduce additional degradation pathways and enhance the rate of degradation. At this time the study of polymer degradation is driven by two major challenges: (1) to understand the mechanism and predict the useful lifetime of polymers in specific applications and (2) to control and stabilize the polymer properties by various additives.

The concept of diffusion-limited oxidation (DLO) developed by Clough and co-workers has greatly contributed to the understanding of the mechanism for polymer degradation: If oxygen diffusion is slow compared to the rate of degradation, as in accelerated degradation in the laboratory, only thin surface layers in contact with air are degraded, while the sample interior is little, if at all, affected; this is the DLO regime.[5] This concept implies that lifetimes of polymeric materials deduced from the study of *average* properties of samples involved in accelerated degradation cannot be used to estimate the durability of polymers in normal exposure. For this reason, methods for measuring the spatial distribution of polymer properties due to degradation have been developed: Density profiling measures the change in density along the irradiation depth, which is expected to increase in aged samples,[6] and modulus profiling measures the tensile modulus, which decreases during degradation.[7,8] The spatial variation of these properties is an excellent indicator of degradation, especially at advanced stages in the degradation process. Both profiling methods are destructive, in the sense that the sample is cut into sections and each section is studied separately.

Hindered amine stabilizers (HAS) are important additives used for light and heat stabilization of polymers. Nitroxides and amino ethers are the major products of reactions involving HAS. The HAS-derived nitroxides are relatively stable but react with free radicals (as "scavengers") to yield diamagnetic species, thus intercepting the degradation cascade. The amino ethers can regenerate the original nitroxide radicals, resulting in an efficient protective effect. So far the complex protection offered by HAS is known only in general terms.[3,9−11]

We have initiated a study of HAS behavior in poly(acrylonitrile−butadiene−styrene) (ABS) exposed to UV radiation, using electron spin resonance (ESR) spectroscopy and ESR imaging (ESRI). Imaging is based on encoding spatial information in the ESR spectra via magnetic field gradients.[12−15] The concentration profiles of HAS-derived nitroxide radicals have been deduced by 1D ESRI as a function of exposure time of the polymer to a Xe source in a weathering chamber.[16] The spatial variation of the nitroxide radicals has been determined by 2D spectral−spatial ESRI of the same samples.[17] These two feasibility studies have demon-

* To whom correspondence should be addressed. E-mail: schlicks@udmercy.edu.

10.1021/ma001719u CCC: $20.00
Published on Web 03/22/2001

Chart 1

(a) Repeat Units in ABS Polymers

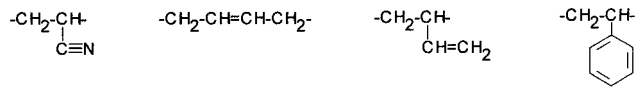

(b) Hindered Amine Stabilizer (HAS): Tinuvin 770

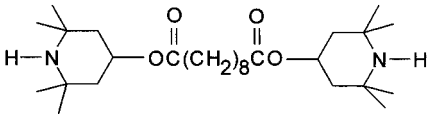

strated that *nondestructive* spectral profiling is possible by ESRI; moreover, this method is sensitive to early events in the degradation process and is therefore expected to be complementary to the density and modulus profiling.

In this paper we compare the behavior of HAS-derived nitroxides in ABS as a result of thermal degradation, UV irradiation with a Xe source that resembled the spectral range and intensity of sunlight, and UV irradiation with fluorescent lamps in the UVB range (290−320 nm). The main motivation for this study was to clarify questions raised in the accelerated degradation by the Xe source[16] and to extend our understanding of the degradation process. In addition, the accelerated rate of ozone depletion in the stratosphere due to environmental factors is expected to raise the level of UVB radiation[18] and to increase the severity of problems associated with polymer deterioration. The present study is expected therefore to have environmental significance.

As will be clearly seen below, the nitroxide signal as a result of UVB irradiation is strong on the irradiated side, but with increasing irradiation time nitroxide radicals appear throughout the sample depth. The effect of UVB radiation is in marked contrast with results obtained by exposure of the same samples to a Xe source; after Xe source irradiation, strong signals from nitroxide radicals were detected at both the irradiated side and the opposite side, and their intensity was very weak in the sample interior.[16,17] The behavior of the nitroxide radicals in the UV-irradiated samples was compared to thermal degradation at 318 and 333 K.

Experimental Section

Sample Preparation. Accelerated degradation experiments were performed by exposure to UV irradiation of poly(acrylonitrile−butadiene−styrene) (ABS Magnum 342 EZ, from Dow Chemical Company) doped with 2% w/w of (bis-(2,2,6,6-tetramethyl-4-piperidinyl) sebacate), the HAS known as Tinuvin 770 from Ciba Specialty Chemicals Corporation (Chart 1). The polymer and the HAS were blended, shredded, and shaped into 10 cm × 10 cm × 0.4 cm plaques in an injection molding machine at 483 K. The plaques were irradiated on one of the large sides in two ways: in a Ci35 Atlas Weather-ometer equipped with a Xe arc that mimicked the solar spectrum and in a UV-2 Atlas Weather-ometer equipped with four fluorescent lamps in the UVB range (FS-20, 290−320 nm). The former irradiation chamber allowed simultaneous control of the temperature (black panel temperature 338 K) and humidity, while the temperature in the latter chamber was 318 K. All plaques were irradiated continuously. For the ESRI experiments, cylindrical samples 4 mm in diameter were cut from the plaques, with the cylinder axis along the direction of the UV radiation. The samples were placed in the ESR resonator with the symmetry axis along the field gradient. Thermal degradation was performed in the irradiation chambers on samples covered with aluminum foil or in a constant-temperature bath at 333 and 318 K. Additional details have been reported.[16,17]

The results reported here are based on the study of 10 plaques, of which seven contained HAS and three were control samples (without HAS). Of the plaques containing HAS two had their backside (not exposed to UV) covered with Al foil and two were entirely covered with Al foil, for thermal degradation in the weathering chambers. In the plaques that contained HAS, a very weak nitroxide signal (concentration $\approx 1 \times 10^{-9}$ mol/g) was detected before irradiation or thermal treatment, but this signal was negligible in comparison with the signal detected in the thermally- or UV-treated samples. At least three samples were examined for each irradiation time in the weathering chamber. Only minor variations in the nitroxide intensity were detected between samples cut at different positions of a given plaque or from different plaques.

Measurement of Nitroxide Concentration. The first step was the preparation of a calibration curve of the ESR intensity vs concentration for standard nitroxide solutions. To this end six solutions of the radical 4-oxo-2,2,6,6-tetramethylpiperidin-1-yloxyl (TEMPONE) (Sigma, purity 95%) in benzene (Sigma-Aldrich, purity 99.9%, HPLC grade) were prepared. The tubes containing the solutions were placed in an outer quartz tube of 5 mm i.d. on which a sample of Mn^{2+} in a single crystal of MgO as internal standard was fixed by Teflon tape. The ESR spectra of the nitroxide samples were measured at 300 K, the signals were doubly integrated, and the value of the integral was plotted as a function of concentration. A good linear plot was obtained for nitroxide concentrations in the range 1×10^{-5}−5×10^{-3} mol/L. The radical concentrations in ABS samples were read from the calibration curve and translated into concentration per unit volume and, from the known sample dimension, into concentration per mass of polymer (mol/g). We estimate a relative error margin in the concentrations of ≈15% and a lower absolute accuracy, ≈30% at best.

Additional information on the line shapes, the relative intensity of the two spectral components, and the absolute intensity of the nitroxide radicals was obtained by measuring sections of the irradiated and thermally degraded cylindrical samples. The sections were obtained by cutting the ABS cylinders typically into five sections, using a regular blade.

ESR Imaging. The ESR imaging system in our laboratory consists of the Bruker 200D ESR spectrometer with an EMX console and equipped with two Lewis coils and two regulated dc power supplies. The coils supply a maximum linear field gradient of ≈320 G/cm in the direction parallel to the external magnetic field or ≈250 G/cm in the vertical direction (along the long axis of the microwave resonator), with a control current of 20 A applied to each coil.[15−17]

1D ESRI. The concentration profile was deduced from two spectra: one in the presence (the 1D image) and one in the absence of the field gradient.[15−17,19,20] The concentration profiles can be deduced by deconvolution of the 1D images; this procedure is correct only if the ESR line shape *has no spatial dependence* along the gradient direction.

Most ESR spectra measured at 300 K after UV or thermal degradation of HAS-containing ABS consisted of two spectral components, from nitroxides differing in their dynamical properties, F ("fast") and S ("slow"), as seen for example in Figure 1. The deconvolution of the ESR spectra into the F and S components has been described.[16] In thermal degradation the intensity ratio of the F and S components was constant through the sample depth, and the concentration profiles were obtained from 1D images and ESR spectra measured at 300 K. In the UV-irradiated samples, however, the ratio of the two spectral components varied with sample depth (vide infra).[17] In these samples the spatial dependence of the line shapes was avoided by deducing the concentration profiles from ESR spectra and 1D images measured at 240 K. At this temperature the two spectral components, F and S, were close to the rigid limit and had identical line shapes. No correction for the sensitivity profile of the ESR cavity was needed because the samples were ≤4 mm long. Most concentration profiles were

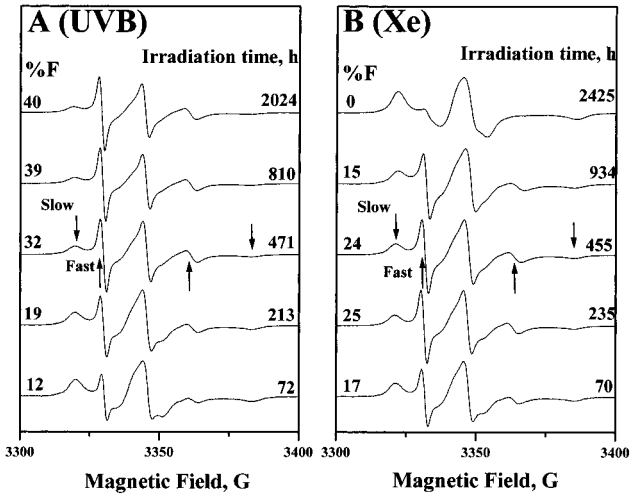

Figure 1. X-band ESR spectra at 300 K of ABS containing HAS for the indicated UV irradiation times with an FS-20 source (UVB) (A) and with a Xe arc (B), in weathering chambers. Upward and downward arrows point respectively to the low- and high-field signals of the "fast" (F) and "slow" (S) spectral components. The percentage of the "fast" component, %F, in each spectrum is indicated.

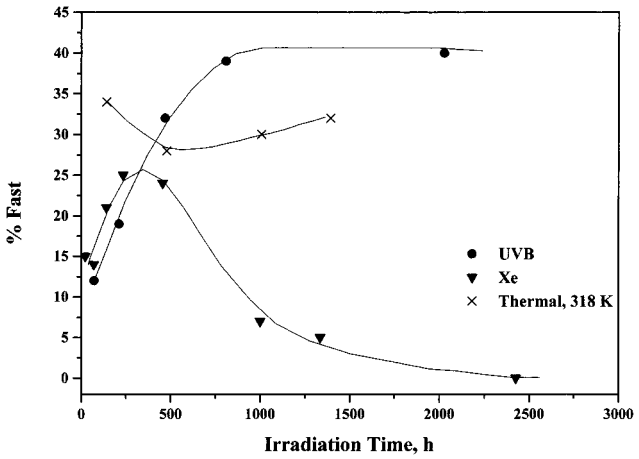

Figure 2. %F determined from ESR spectra of whole samples measured at 300 K as a function of irradiation time with the UVB and Xe sources and for thermal degradation at 318 K. Solid lines were drawn by nonlinear regression.

determined from spectra measured with gradients in the range 100−200 G/cm.

2D ESRI. Each 2D spectral−spatial image was reconstructed from a set of projections collected as a function of the magnetic field gradient.[12,15,17,21] The maximum experimentally accessible projection angle, α_{max}, is determined by the maximum gradient G_{max}: $\tan \alpha_{max} = (L/\Delta H)G_{max}$, where L is the spatial dimension and ΔH is the spectral width. For a spectral width $\Delta H \approx 69$ G, which was dictated by the slow-motional spectral component (S), a sample length of 0.4 cm, and a maximum field gradient of 250 G/cm, $\alpha_{max} = 56°$, and $SW_{max} = 175$ G. A set of data typically consisted of 128 projections, taken for gradients corresponding to equally spaced increments of α in the range −90° to +90°; of these projections, 83 were experimentally accessible, and the rest were projections at missing angles. Each projection required 1−9 scans, and each scan was obtained with scan time 41 s, microwave power 2−6 mW, modulation 0.5−2 G, time constant of 20−41 ms, and gain 1×10^3−2×10^5.

The reconstruction of the 2D image was based on the back-projection algorithm,[21] modified[22] to include the projection slice algorithm (PSA).[23] The image reconstruction procedure consisted of three major modules: The first module performs a variety of procedures, including the handling of the missing projections. Two initial choices for the missing projections are possible: these projections can be set equal to zero or equal to the projection measured at α_{max}; we chose the latter option. The second module computes the image from the projections measured at the corresponding angle α, using the filtered back-projection algorithm. This module includes a choice of filters designed directly for the frequency domain. The third module initiates the iteration process for the missing projections.

The reconstruction algorithm produced 2D images on a 256 × 256 grid. This file size is convenient in terms of computational speed, viewing of images, and display of spatial and spectral details.

Results

ESR Spectra at 300 K. Selected X-band ESR spectra at 300 K of the HAS-derived nitroxide in ABS, for the indicated irradiation times in the weathering chamber, are shown in Figure 1A for the UVB source and in Figure 1B for the Xe source. All spectra, except that corresponding to the longest irradiation time in Figure 1B, consist of a superposition of two components, from nitroxide radicals differing in their mobility: a "fast" component (F) with a total width of ≈32 G and a "slow" component (S) with a spectral width of ≈64 G. The corresponding rotational correlation times, τ_c, are 4×10^{-9} and 5×10^{-8} s/rad, respectively, deduced by simulations of the spectra.[16] The spectra indicate the presence of HAS-derived nitroxides in two different environments. It is reasonable to assign the fast and slow components to nitroxides located respectively in low-T_g domains dominated by polybutadiene sequences ($T_g \approx 200$ K) and in high-T_g domains dominated by polystyrene ($T_g \approx 370$ K) or polyacrylonitrile sequences ($T_g \approx 360$ K).

The two spectral components, F and S, were also detected in the ESR spectra measured at 300 K for HAS-containing ABS samples that were covered with Al foil and kept in the weathering chambers or thermally degraded in a constant-temperature bath maintained at the temperature in the weathering chambers.

The ESR spectrum corresponding to the F component was isolated by subtracting the spectrum of the slow component presented at the top of Figure 1B from one of the composite spectra. After this step it was easy to superimpose the two components and to reproduce all composite spectra; the relative concentration of each spectral component was then obtained by double integration. After examination of numerous samples we became convinced that the F and S components in the different samples are identical, and the various composite spectra differ only in the relative intensity of the two components. The percentage of the fast component, %F, calculated as described above, is given for all spectra shown in Figure 1.

The variation of %F with time of UV irradiation by the two sources and of thermal treatment at 318 K is presented in Figure 2. The relative intensity of the F component as a function of irradiation time with the Xe arc increases to a maximum, decreases, and becomes negligible at the longest irradiation time, 2425 h. For UVB irradiation, however, %F increases and reaches a plateau at $t \approx 1000$ h. For thermal degradation the variations in the %F with heating time are not very pronounced, as clearly seen in Figure 2 for treatment at 318 K. For samples heated at 333 K, %F increases to 35% after 1947 h of heating and decreases to 14% after 4600 h of heating.

Concentration of Nitroxide Radicals. The concentration of nitroxide radicals, [NO•], in the cylindrical

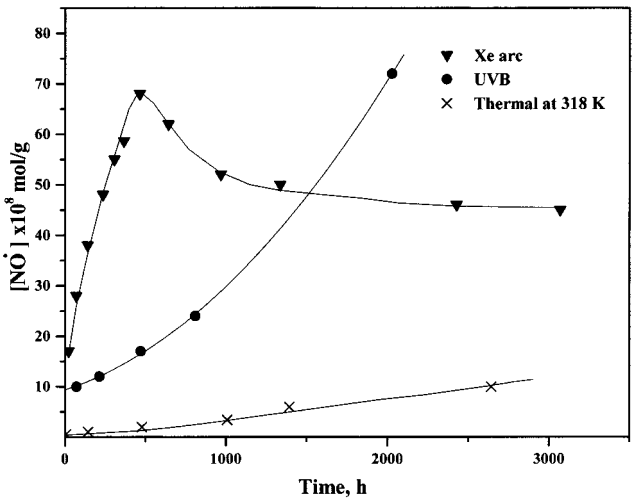

Figure 3. Concentration of HAS-derived nitroxide radicals, [NO•], in UV-irradiated and thermally degraded ABS. Solid lines were drawn by nonlinear regression.

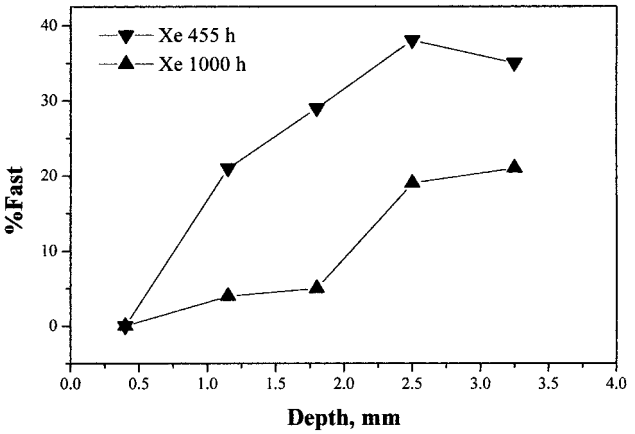

Figure 4. %F vs depth for two irradiation times with the Xe arc, 455 and 1000 h. Data are based on sectioned samples.

samples as a function of time of UV irradiation and thermal degradation is given in Figure 3. The concentrations were determined as described in the Experimental Section.

Even before performing the ESR imaging experiments, we deduced by sectioning of some samples that the radical concentration varies along the sample depth (from the irradiated side) in Xe arc irradiation but is constant with sample depth in thermal degradation. Moreover, the %F as a function of depth for Xe irradiation depends on the irradiation time, as seen in Figure 4 for irradiation times of 455 and 1000 h in the weathering chamber. This spatial variation of the line shapes dictated the lower temperature, 240 K, for the measurements of the ESR spectra and 1D images, as will be seen below.

Radical Profiles from 1D ESRI. The concentration profiles of nitroxide radicals in ABS along the irradiation depth are given in Figure 5A for UVB irradiation and in Figure 5B for Xe arc irradiation, at the indicated irradiation times. The profiles are spatially inhomogeneous in both cases. The strong nitroxide concentration at the backside of the samples irradiated with the Xe source was also obtained when this side was covered with Al foil, indicating that the radicals present on this side are not due to direct irradiation, for instance by scattered light.[17]

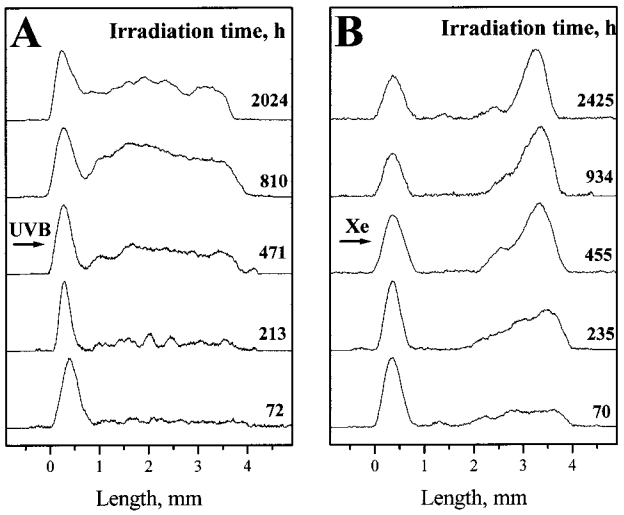

Figure 5. Concentration profiles of HAS-derived nitroxides obtained by deconvolution of 1D ESRI images measured at 240 K, for the indicated UV irradiation times of ABS in the weathering chamber: (A) UVB irradiation, 1D image measured with $G_x = 177$ G/cm; (B) Xe arc irradiation, 1D image measured with $G_x = 152$ G/cm. The horizontal arrow indicates the irradiated side of the sample.

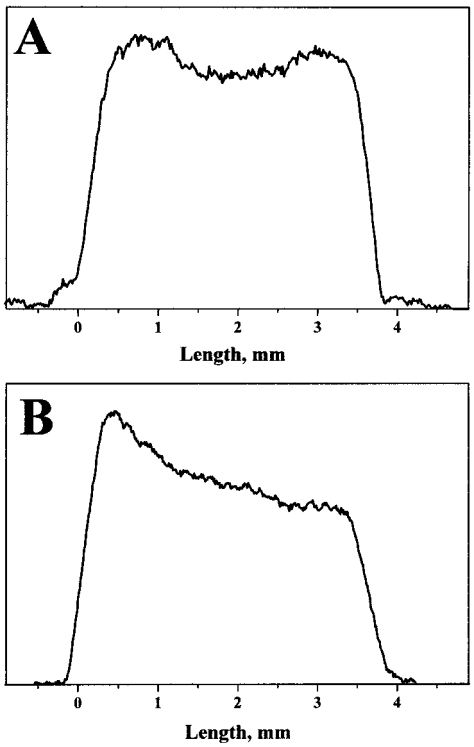

Figure 6. Concentration profiles of HAS-derived nitroxides obtained by deconvolution of 1D ESRI images measured at 300 K, for thermal degradation of ABS in the weathering chamber: (A) for ABS samples covered with Al foil and kept in the UV-2 weathering chamber behind an Al screen for 471 h during UVB irradiation; (B) for ABS samples covered with Al foil and kept in the weathering chamber for 643 h during Xe arc irradiation. The gradient was 102 G/cm.

Figure 6A shows the concentration profiles for ABS plaques covered with Al foil and kept in the weathering chamber for 471 h at 318 K during UVB irradiation. The nitroxide distribution is almost completely homogeneous; to prevent a temperature gradient in the chamber, the sample was kept behind, and at a distance of ≈1 cm from, an Al screen that faced the UVB source.

The concentration profiles for ABS plaques completely covered with Al foil and kept in the weathering chamber for 643 h at the black panel temperature of 338 K during Xe irradiation are shown in Figure 6B. The nitroxide distribution is similarly homogeneous; the slightly higher radical concentration on the side facing the UV source is attributed to a temperature gradient in the chamber. Indeed, samples kept in the constant-temperature bath at 333 K (to reproduce the average temperature of the sample in the weathering chamber) exhibited a homogeneous radical distribution.

2D Spectral−Spatial ESRI. The spatial variation of the two spectral components, F and S, was obtained from 2D spectral−spatial ESRI measurements, and the results of UV exposure (with the Xe and UVB sources) were compared with the results of thermal degradation. Figure 7 presents 2D spectral−spatial perspective and contour images of nitroxide radicals in ABS UV-irradiated in the weathering chamber by the UVB source for 72 h (Figure 7A) and for 810 h (Figure 7B). The 2D images for samples irradiated with the Xe source are shown in Figure 8 for 70 h (Figure 8A) and for 643 h (Figure 8B). The ESR intensity is presented in the absorption mode. On the right side of Figures 7 and 8 are "virtual" slices (in the derivative mode) obtained *nondestructively* at the indicated depths of the sample. The spectral slices indicate not only the line shape variation but also the relative intensity of each spectral component as a function of depth. For the short irradiation time ($t = 70$ h) by the Xe arc the ESR spectrum of the directly irradiated part of the sample exhibits a composite spectrum with %F = 42; at and near the nonirradiated side %F is significantly larger, 63%. After 643 h of irradiation, the irradiated side contains no fast component, and %F decreased significantly at and near the nonirradiated side. Section "b" in Figure 8B represents a very weak signal, and %F was not calculated for this section. It is important to note the similarity of the spectra in the directly irradiated layer for the two UV sources at longer irradiation times, 643 h for Xe arc and 810 h for UVB irradiation. At short irradiation times (≈70 h), however, %F is ≈42% for Xe arc and ≈3% for UVB irradiation.

The contrasting behavior of thermally degraded samples is clearly seen in Figure 9, for ABS thermally degraded and kept covered in the weathering chamber at 318 K for 478 h. Not only is the spatial distribution of the nitroxide radicals spatially homogeneous, but no spatial variation of the line shapes was observed, and on the average %F = 26 ± 4%.

Examples of the exquisite details that can be deduced from 2D spectral−spatial ESRI are shown in Figure 10: The evolution of %F along the sample depth as a function of irradiation time is in Figure 10A for the UVB source ($t = 72$ and 810 h) and in Figure 10B for the Xe source ($t = 70$ and 643 h). The plots do not include data for the Xe arc at depth range 0.5−1.7 mm because the intensity of the signal is too low, and the margin error in %F is too large.

Discussion

In this section we will examine the degradation process in the different domains from an analysis of the ESR spectra, make deductions on the difference between thermal and UV degradation from the ESR and ESRI results, consider the relative intensity of the F and S components and the absolute concentration of the nitroxide radicals in terms of the initial HAS content, and comment on the development of our ideas on degradation and on remaining questions that need to be addressed in the future.

Degradation in Morphologically Distinct ABS Domains. The nitroxide radicals formed from the HAS are not only indicators of the reactions that take place during UV and thermal degradation but also reporters of the polymer morphology. Deductions on morphology are based on the temperature variation of the ESR line shapes, ^{14}N hyperfine splittings, and the specific motional mechanism that can be deduced from simulation of the spectra.[24−28] The variation of the intensity ratio of the two spectral components, F and S, in the ESR spectra shown in Figure 1 reflects therefore a complex combination of local morphology and chemical processes.

If we are interested in ABS morphology, it is advantageous to study the early stages of UV and thermal degradation. We note that %F can be deduced with high accuracy because of the narrow ESR signals and the high corresponding amplitudes. The fact that this component appears clearly only in ESR spectra measured at and above 260 K suggests that the F component represents a low-T_g domain.[29,30] The results presented in Figures 1−3 show that %F, a spectral component identified with the butadiene-rich domains, is the minor component in the early stages of UV degradation, <15%. In thermal degradation %F is higher, typically 30% on the average.

If the relative intensity of the F component in the earliest stages of heating or UV irradiation reflects the ABS morphology, the variation of the relative intensity of this component with sample treatment must be taken as an indication of degradation and stabilization reactions in specific morphological domains.

In Xe arc irradiation %F increases to a maximum of ≈25% for irradiation times in the range 250−500 h, decreases above $t \approx 500$ h, and is negligible for $t = 2425$ h. For the same irradiation conditions the total nitroxide concentration decreases above $t = 500$ h from $\approx 70 \times 10^{-8}$ to $\approx 50 \times 10^{-8}$ mol/g; in the same time interval %F decreases from 25% to 0%. From these observations we can conclude that the decrease of the total nitroxide concentration is due mainly to the disappearance of the F component. Therefore, the fate of the F component is representative of the degradation process. This is reasonable, as the F component represents butadiene-rich domains, and the butadiene component in ABS is the most vulnerable to degradation.[31]

The conclusion that the chemical events occur predominantly in the domains with a lower T_g is reasonable, because degradation reactions depend not only on the formation of reactive intermediates but also on their mobility in the polymer matrix. Our study of peroxy radicals produced by γ irradiation of polypropylene has revealed the presence of radicals in both the amorphous and the crystalline regions of the polymer, but the lifetime of the radicals in the amorphous phase is shorter.[32] In ABS the low T_g combined with the double bonds in the butadiene segments defines the most vulnerable regions.

The sectioning experiments presented in Figure 4 are supportive of the conclusion that %F along the sample depth decreases with increasing irradiation time (Xe arc) and is negligible on the directly irradiated side for $t \geq 455$ h. These conclusions will be emphasized in the ESR imaging experiments. The disappearance of the F

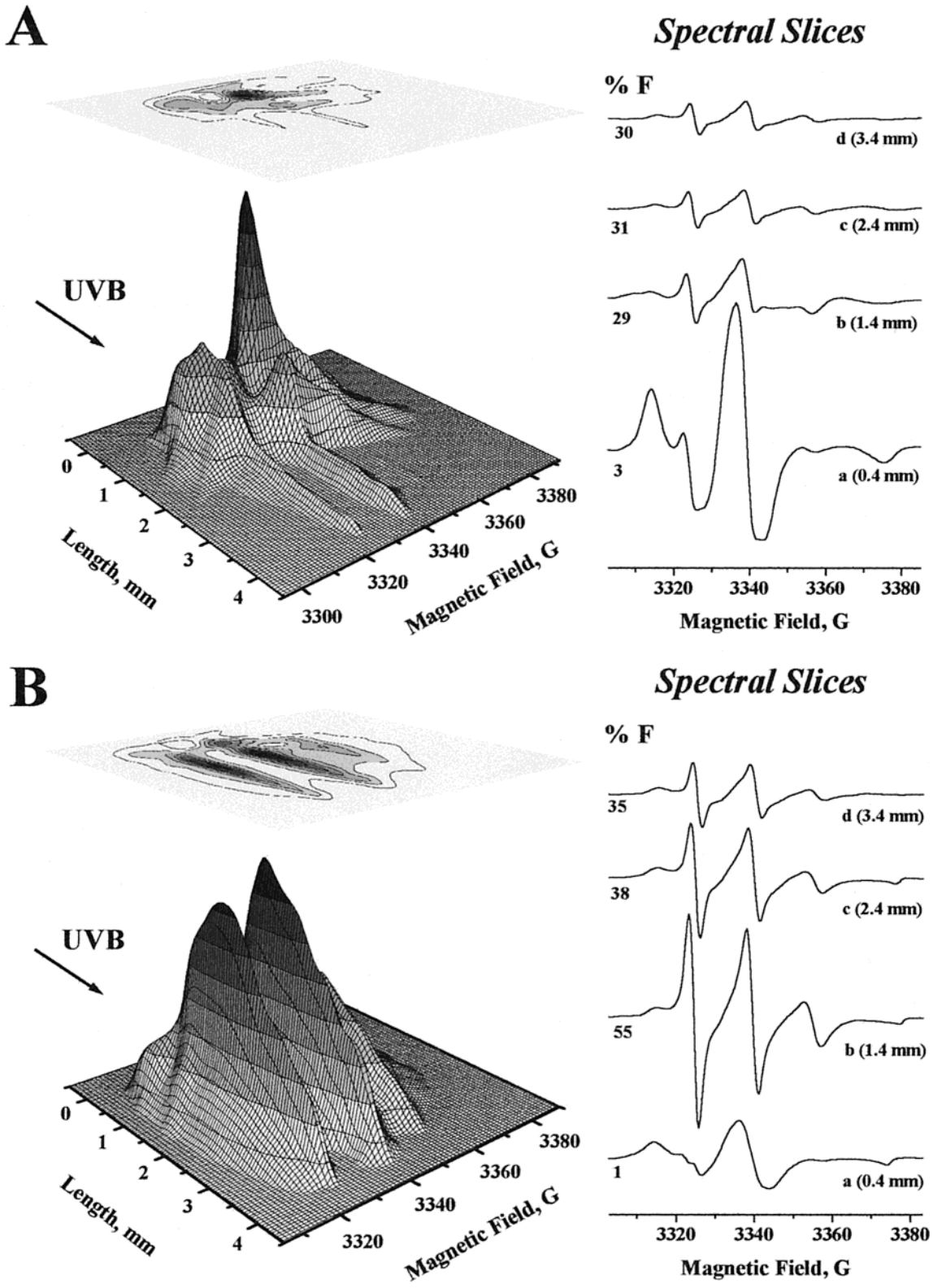

Figure 7. 2D spectral−spatial contour (top) and perspective (bottom) plots of HAS-derived nitroxides after 72 h (A) and 810 h (B) of UVB irradiation in the weathering chamber, presented in absorption. The spectral slices a, b, c, and d for the indicated depths are presented in the derivative mode; these slices were obtained from digital (nondestructive) sections of the 2D image. %F is shown for a, b, c, and d slices. Both 2D images were reconstructed from 83 real projections, Hamming filter with $D = 0.45$, two iterations, $L = 4.5$ mm, and $\Delta H = 69$ G and were plotted on a 256 × 256 grid.

spectral component can also occur due to major changes in the butadiene segments, for instance because of cross-linking. In this case the nitroxide signals would represent a higher T_g, and the extreme separation would increase, perhaps even becoming similar to that of the S component. Taken together, the data presented in Figures 1−4 suggest therefore that the temporal and spatial variation of the intensity of the F spectral component is an indicator of both morphology and degradation.

Mechanism of UV and Thermal Degradation. We will first discuss the results of irradiation by the Xe arc

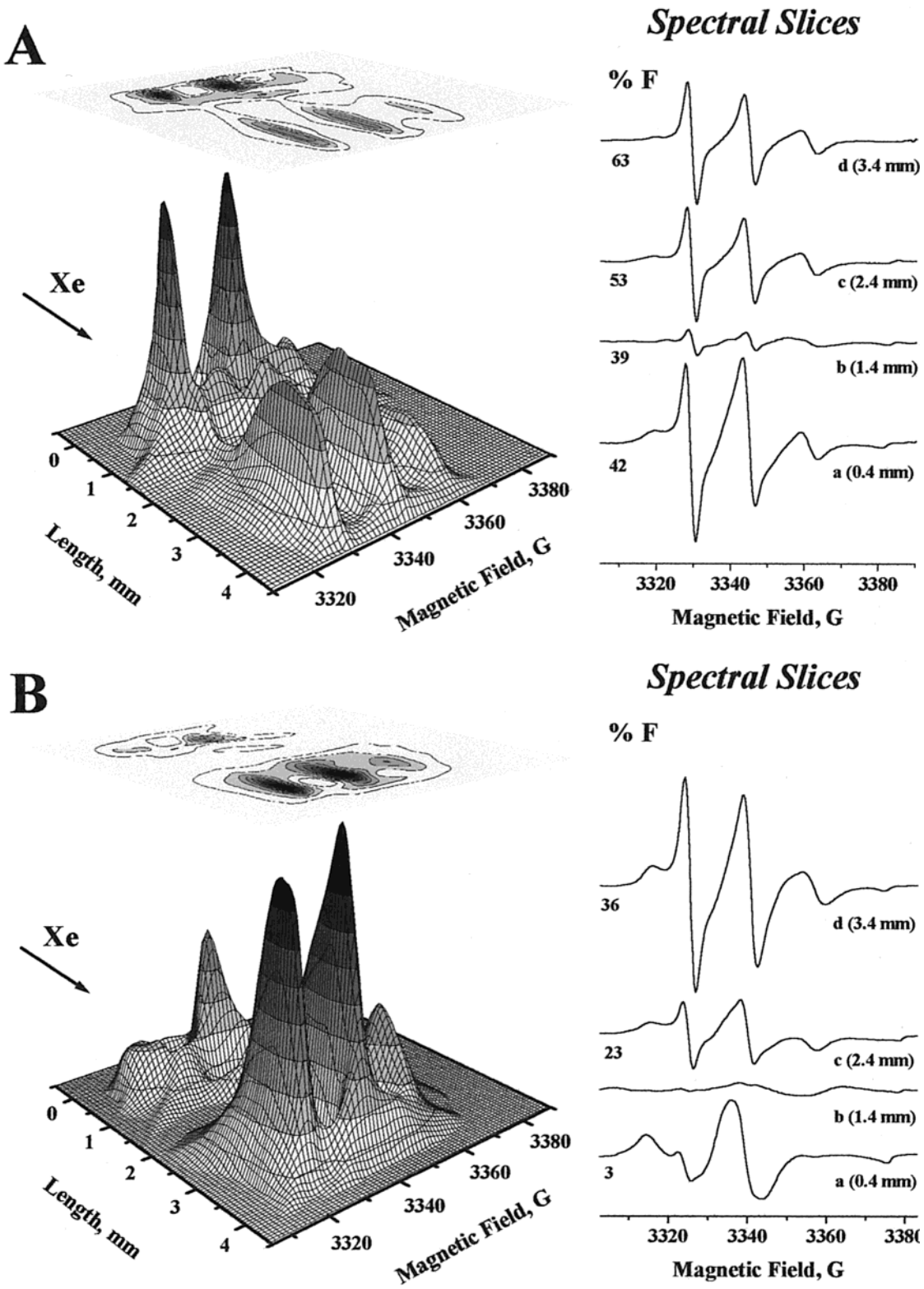

Figure 8. 2D spectral−spatial contour (top) and perspective (bottom) plots of HAS-derived nitroxides after 70 h (A) and 643 h (B) of irradiation by the Xe arc in the weathering chamber, presented in absorption. The spectral slices a, b, c, and d for the indicated depths are presented in the derivative mode; these slices were obtained from digital (nondestructive) sections of the 2D image. %F is shown for a, b, c, and d slices in (A) and for a, c, and d slices in (B). Both 2D images were reconstructed from 83 real projections, Hamming filter with $D = 0.45$, two iterations, $L = 4.5$ mm, and $\Delta H = 70$ G and were plotted on a 256 × 256 grid.

in the weathering chamber. The concentration profiles deduced from 1D ESRI indicate a strong radical concentration on the irradiated side at low irradiation times and progressive appearance of a strong signal on the opposite side (Figure 1B); these profiles reflect inhomogeneous degradation. The signal on the irradiated side is located in a narrow layer, <1 mm; the exact thickness is difficult to estimate, because the ESRI resolution is expected to be only ≈0.3 mm. In the sample interior the radical intensity is very low.

Spatially inhomogeneous polymer degradation has been reported before. In polymer samples degraded at

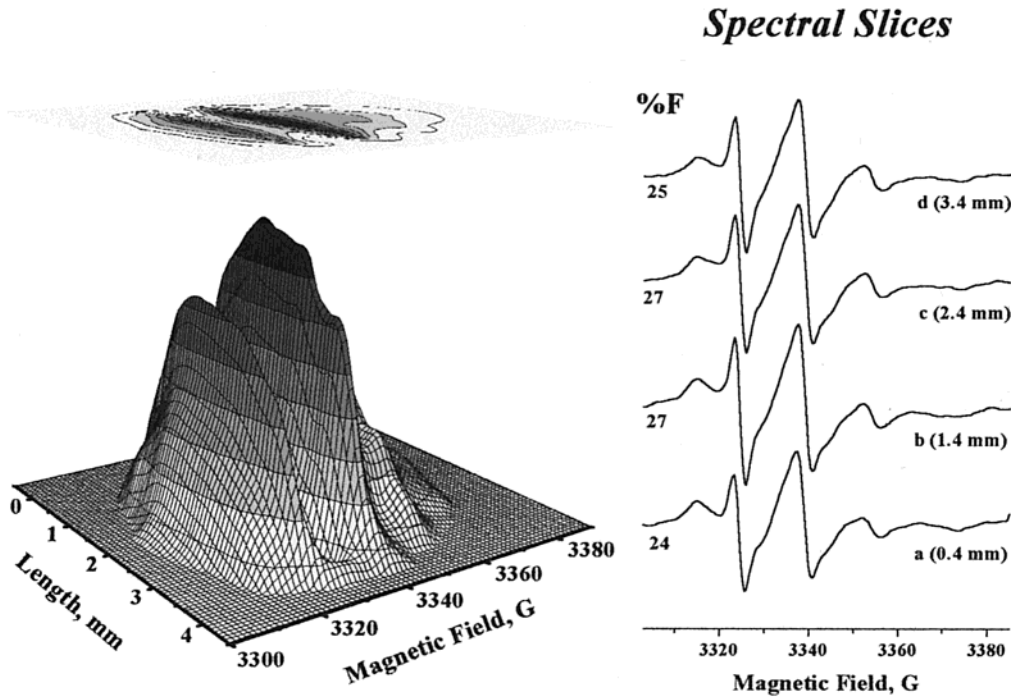

Figure 9. 2D spectral−spatial contour (top) and perspective (bottom) plots of HAS-derived nitroxides after thermal degradation for 78 h at 318 K, presented in absorption. The spectral slices a, b, c, and d for the indicated depths are presented in the derivative mode; these slices were obtained from nondestructive sections at the indicated position. The 2D image was reconstructed from 42 real projections, Hamming filter with $D = 0.45$, two iterations, $L = 4.1$ mm, and $\Delta H = 70$ G and was plotted on a 256 × 256 grid.

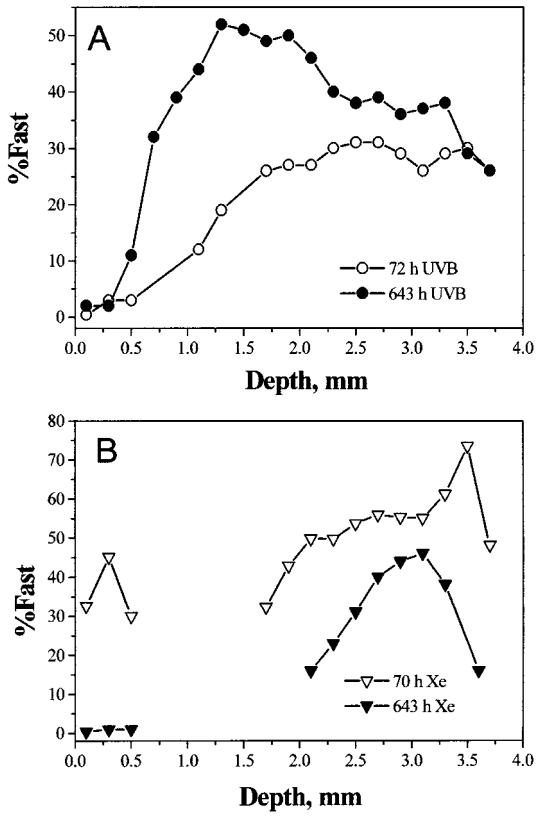

Figure 10. %F as a function of depth for the indicated irradiation times: (A) UVB source; (B) Xe arc. Data are deduced from digital (nondestructive) sectioning of the 2D spectral−spatial ESR images, such as those presented in Figures 7 and 8; see text.

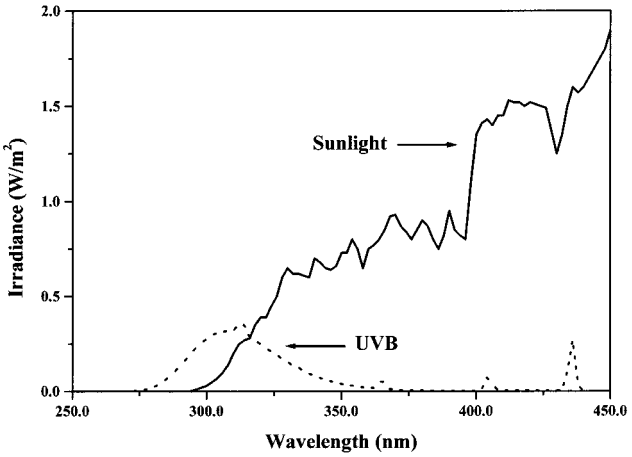

Figure 11. Irradiance as a function of wavelength for sunlight and the UVB (FS-20) source.

relatively elevated temperatures (80−150 °C) or exposed to high-energy radiation (γ rays), profiling methods have revealed significant changes in modulus, density, and carbonyl index only in the outer layers in contact with oxygen; these variations have been rationalized by the DLO concept.[5−8,33−35] Because in these systems the temperature is constant along the sample depth and γ rays penetrate through the entire depth, inhomogeneous degradation is a manifestation of DLO.

Inhomogeneous degradation has also been observed in UV-irradiated polymers. In the case of polypropylene this phenomenon has been detected by 1D ESRI for polymer irradiation with a Xe arc[36] and by FTIR ("carboxyl index"), molecular mass, and crystallinity of sections for irradiation with UVA light.[37,38] The inhomogeneity is more difficult to explain in these experiments, because the $\lambda < 300$ nm radiation, which is absorbed by the polymer, is expected to penetrate only in a thickness of ≤ 50 μm.[31] Moreover, UVA light has significant intensity only for wavelengths above the absorption wavelength of polypropylene. Therefore, while a weak nitroxide signal is expected on the non-irradiated side, comparable to nitroxide concentration

due to heating, the high nitroxide concentration on the nonirradiated side, even in samples whose back was covered with Al foil, needs an explanation.[16]

The results for the ABS samples irradiated by the UVB source helped to clarify this question. Comparison of the spectra ranges for the two UV sources is shown in Figure 10; while the UV range 290−320 nm for the FS-20 lamps is intense, this source lacks the spectral range above 350 nm.

Inspection of the ESR spectra and concentration profiles, Figures 1 and 5, indicates major differences between the results obtained for the two UV irradiation sources. First, the strong nitroxide signal on the back of the sample is not seen for the UVB source; instead, the radical concentration increases with irradiation time, and the radical is present throughout the sample. Second, the F component is intense through the entire sample (with the exception of the directly irradiated layer), as expected for thermal degradation. Third, %F is high in the UVB-irradiated samples, even for irradiation time ≥2000 h. We note that for long irradiation time (2425 h) %F was negligible in the Xe irradiation (Figure 1B).

Formation of nitroxide radicals is a facile reaction: the radicals were detected by heating to relatively low temperature, 318 K. The radicals are present, albeit in very small concentration, even in samples that were kept at or below ambient and not exposed to UV light. Therefore, the disappearance of the F component upon extended Xe arc exposure must be associated with scavenging of reactive radicals, formation of amino ethers, and consumption of nitroxide radicals by other reactions. A direct result of this conclusion is that in the UVB experiments significant consumption of nitroxide radicals due to stabilization occurs on the irradiated side only, while in the case of Xe radiation, the F nitroxides are consumed throughout the sample depth.

At this point it seems reasonable to assume that the range of the Xe arc above 350 nm is responsible, at least in part, for the high nitroxide concentration on the back of the sample. Because the components in neat ABS do not absorb in this range, we must implicate chromophores present as impurities or even HAS and the HAS-derived nitroxides as absorbers in the visible. Indeed, the degradation of ABS with light of $\lambda > 400$ nm is extensive.[39,40] In addition, different temperature and humidity conditions during irradiation are also important factors.

The profiles shown in Figure 5B exhibit an additional case of diffusion-limited oxidation: significant degradation occurs by UV light (on the irradiated side) and by visible light (on the back of the sample) and less in the sample interior.

Thermal degradation at 318 and 333 K is a very slow process during 2000 h of treatment. In this time interval the distribution of the nitroxide radicals is homogeneous, and %F is constant with time. The decrease of %F to 14% after heating for 4600 h at 333 K shows the slower time scale for thermal degradation, compared to UV degradation. For thermal degradation at 318 K the expected rise and fall of %F have not been detected yet during 2000 h of treatment.

We will now examine the variation of %F with sample depth and will begin with UVB data (Figure 10A). For $t = 72$ h the average %F is 12% as seen in Figure 1A. In the thin irradiated layer, ≤0.5 mm, however, %F is ≈0 and reaches a maximum of ≈30% in the center of the sample. We note that the total nitroxide intensity at depth 0.5−1.0 mm is low, and it is difficult to deduce %F. For $t = 810$ h, the intensity of the F component is negligible on the irradiated side (as for $t = 72$ h); the maximum intensity of F is higher, ≈50%, but decreases toward the opposite side. Data in Figure 10A indicate clearly the progress of degradation and stabilization on the directly irradiated side where %F is ≈0 even at low irradiation times, the progressive increase of %F in the center due to slower thermal degradation and DLO, and the decrease of % F on the opposite side due to consumption of nitroxides in the stabilization process.

The depth variation of %F during Xe arc irradiation tells us a different story. The decrease of %F to ≈0 is not seen for $t = 70$ h (as in UVB radiation) but is seen at $t = 643$ h, and even at $t = 455$ h as seen in Figure 4, and shows the consumption of the F nitroxide component in the irradiated layer. Together with the top spectrum in Figure 1B, which shows %F ≈ 0 in the entire sample for $t = 2425$ h, data for Xe arc irradiation predict progressive consumption of nitroxides through the entire sample depth during ≈2000 h.

In the case of thermal degradation, %F is constant with depth for a given degradation time but varies with time. For this situation, spectral profiling is completely determined by the data shown in Figures 2, 3, and 6. The 2D ESRI experiments, one of which is presented in Figure 9, reinforce the conclusions deduced from ESR spectra and 1D ESRI experiments.

Concentration of HAS-Derived Nitroxides. The nitroxide concentration in whole samples (Figure 3), the intensity profiles deduced from 1D ESRI (Figures 5A and 5B), and the spatial variation of the F and S components deduced from 2D spectral−spatial ESRI (Figures 7−9) allow the complete mapping of the nitroxide radicals with time and sample depth; this is spectral profiling. The data obtained in this study also allow to establish a correlation between the nitroxide radicals and the original HAS content in the ABS samples.

The initial Tinuvin content, 2% w/w, corresponds to a concentration of 4×10^{-5} mol/g. The maximum nitroxide concentration measured, 80×10^{-8} mol/g, represents only ≈2% of the initial HAS concentration. This is the situation in the case of thermal degradation, where the nitroxide distribution is spatially homogeneous. The situation can be markedly different, however, if the nitroxide distribution is not homogeneous, as detected for the UV-irradiated samples. If, for example, we consider the nitroxide distribution at $t = 1000$ h, we can assume that roughly half of the radicals are on each side for Xe irradiation, as seen in Figure 5B. If we make the additional reasonable assumption that the nitroxides are localized in a layer of ≈0.1 mm on each side, the nitroxide concentration in this thin layer corresponds to ≈40% of the initial HAS. We can conclude that the distribution of HAS becomes inhomogeneous through the sample depth during UV degradation, because in different regions of the sample the rate of HAS-derived nitroxide consumption is different.

But there is a more subtle type of nitroxide and HAS heterogeneity, which is a result of the polymer morphology: If we consider only the HAS-derived nitroxide radicals present in the outer layers in the low-T_g domains (the F component), we can approach a nitroxide concentration quite similar to that of the original HAS.

Therefore, the HAS is consumed more rapidly, and its concentration decreases faster in the butadiene-rich domains compared to the high-T_g domains dominated by styrene and acrylonitrile sequences. The absence of the F component in the irradiated layer can be therefore considered a result of the consumption of all HAS in the butadiene-rich domains. This is the case for Xe irradiation after $t > 455$ h and for UVB irradiation even after 70 h.

It seems that during UV irradiation a hierarchical distribution of HAS eventually emerges during 2000 h of irradiation: heterogeneity on the scale of micrometers because of the polymer morphology and on the scale of millimeters because of the spatial dependence of degradation processes. In thermal degradation only the morphological heterogeneity is detected, as expected.

Additional Comments. In support of the conclusions described above we can mention preliminary annealing results. Two types of annealing phenomena were observed. First, after irradiation with the Xe arc for ≈2000 h, we detected the reappearance of the F component in samples left at ambient temperature for several months, typically 6 months. Second, during measurement of the temperature dependence of the ESR spectra we noticed an increase in the %F at 300 K after heating of ABS samples to 400 K for typically ≈30 min. Both phenomena can be explained by migration of HAS-derived nitroxides from the high-T_g domains to the low-T_g domains. The acceleration of annealing by heating of ABS samples to 400 K, near the T_g of the styrene and acrylonitrile sequences, seems to reinforce the idea of interdomain nitroxide migration.

The time scale for the nitroxide migration can be roughly estimated from the diffusion coefficient of the HAS, D(HAS). A reasonable estimate is 1×10^{-10} cm^2 s^{-1}.[41] The mean-square displacement in simple Brownian motion in one dimension is $\langle x^2(t) \rangle = 2Dt$. The displacement is <0.5 mm for $t = 2000$ h, which is the longest time in our UV experiments. Therefore, we tentatively conclude that in the annealing experiments we observed only interdomain displacement and not displacement along the sample depth. In contrast to the slow transport rate of HAS and nitroxides through the sample depth, the oxygen transport, with $D(O_2) \approx 1 \times 10^{-7}$ cm^2 s^{-1}, is significant on the time scale of the irradiation experiments.

Conclusions

Thermal and UV degradation of poly(acrylonitrile−butadiene−styrene) (ABS) containing a hindered amine stabilizer (HAS) was studied by electron spin resonance (ESR) spectroscopy and ESR imaging (ESRI). The intensity profiles of HAS-derived nitroxides were determined by 1D ESRI, and the spatial variation of the ESR line shapes was determined by 2D spectral−spatial ESRI. Together with the determination of the nitroxide concentration, the imaging data allowed the mapping of the temporal and spatial variation of the nitroxides depending on the irradiation source, treatment time, and temperature.

The UV light was provided by fluorescent lamps with maximum intensity in the range 290−320 nm (UVB) or by a Xe arc that closely mimicked the solar spectrum. Upon UVB irradiation the nitroxide signal was initially strong only on the irradiated side and increases with time through the sample. These results were taken as evidence for extensive damage on the irradiated side and slower thermal degradation in the entire sample. The effect of UVB radiation was in marked contrast with that of a Xe source; after such irradiation the nitroxide radicals were detected at both the irradiated side and the opposite side, and their intensity was weaker in the sample interior. Spatial variation of the ESR lines was observed for irradiation with both UV sources. In contrast with UV irradiation, the spatial distribution of the nitroxide radicals was homogeneous during thermal degradation and 318 and 333 K, and there was no spatial variation of the ESR line shapes. The results provided mechanistic details on the early stages of the degradation process.

This study has indicated a hierarchical variation of the HAS-derived nitroxide concentration: within the morphological domains of ABS on the scale of a few micrometers and within the sample depth on the scale of millimeters.

Acknowledgment. This study was supported by the Polymers Program of the National Science Foundation. We thank J. L. Gerlock (Ford Research Laboratory, Dearborn, MI) for his help in the preparation of the ABS plaques and for numerous illuminating discussions and Antonin Marek (Institute of Macromolecular Chemistry, Prague, Czech Republic) for implementation of the Projection Slice Algorithm (PSA) for image reconstruction in 2D ESRI. The authors are grateful to one reviewer for his careful reading of the manuscript and excellent suggestions. S. Schlick is grateful to Gian Franco Pedulli for his hospitality during her sabbatical stay in Bologna, Italy, where this manuscript was revised.

References and Notes

(1) Hill, D. J. T.; Le, T. T.; O'Donnell, J. H.; Perera, M. C. S.; Pomery, P. J. In *Irradiation of Polymeric Materials: Processes, Mechanisms, and Applications*; Reichmanis, E., Frank, C. W., O'Donnell, J. H., Eds.; American Chemical Society: Washington, DC, 1993.
(2) O'Donnell, J. H. In *The Effects of Radiation on High-Technology Polymers*; Reichmanis, E., O'Donnell, J. H., Eds.; American Chemical Society: Washington, DC, 1989; Chapter 1, p 1.
(3) *Polymer Durability: Degradation, Stabilization and Lifetime Prediction*; Clough, R. G., Billingham, N. C., Gillen K. T., Eds.; Adv. Chem. Ser. 249; American Chemical Society: Washington, DC, 1996.
(4) *Handbook of Polymer Degradation*; Hamid, S. H., Amin, M. B., Maadhah, A. G., Eds.; Marcel Dekker: New York, 1992.
(5) Gillen, K. T.; Clough, R. L. *Polymer* **1992**, *33*, 4359.
(6) Gillen, K. T.; Clough, R. L.; Dhooge, N. J. *Polymer* **1986**, *27*, 225.
(7) Gillen, K. T.; Clough, R. L.; Quintana, C. A. *Polym. Degrad. Stab.* **1987**, *17*, 31.
(8) Gillen, K. T.; Clough, R. L.; Wise, J. In *Polymer Durability: Degradation, Stabilization and Lifetime Prediction*; Clough, R. G., Billingham, N. C., Gillen K. T., Eds.; Adv. Chem. Ser. 249; American Chemical Society: Washington, DC, 1996; Chapter 34, p 557.
(9) Gerlock, J. L.; Bauer, D. R.; Briggs, L. M. *Polym. Deg. Stab.* **1986**, *14*, Part I, p 53; Part II, p 73; Part III, p 97.
(10) Pospisil, J. *Adv. Polym. Sci.* **1995**, *124*, 87.
(11) Brede, O.; Beckert, D.; Windolph, C.; Gottinger, H. A. *J. Phys. Chem. A* **1998**, *102*, 1457.
(12) *EPR Imaging and in vivo EPR*; Eaton, G. R., Eaton, S. S., Ohno, K., Eds.; CRC Press: Boca Raton, FL, 1991.
(13) Freed, J. H. *Annu. Rev. Biophys. Biomol. Struct.* **1994**, *23*, 1.
(14) Smirnov, A. I.; Belford, R. L.; Morse, R. *Concepts Magn. Reson.* **1999**, *11*, 277.
(15) Schlick, S.; Eagle, P.; Kruczala, K.; Pilar, J. In *Spatially Resolved Magnetic Resonance: Methods, Materials, Medicine, Biology, Rheology, Ecology, Hardware*; Blümler, P., Blümich, B., Botto, R., Fukushima, E., Eds.; Wiley-VCH: Weinheim, 1998; Chapter 17, p 221, and references therein.

(16) Motyakin, V. M.; Gerlock, J. L.; Schlick, S. *Macromolecules* **1999**, *32*, 5463.
(17) Kruczala, K.; Motyakin, V. M.; Schlick, S. *J. Phys. Chem. B* **2000**, *104*, 3387.
(18) McKenzie, R.; Connor, B.; Bodeker, G. *Science* **1999**, *285*, 1709.
(19) Lucarini, M.; Pedulli, G. F.; Borzatta, V.; Lelli, N. *Polym. Degrad. Stab.* **1996,** *53*, 9.
(20) Ahn, M. K.; Eaton, S. S.; Eaton, G. R.; Meador, M. A. B. *Macromolecules* **1997**, *30*, 8318.
(21) Kweon, S.-C. M.Sc. Thesis, University of Detroit Mercy, 1993.
(22) Marek, A., unpublished work from this laboratory, 2000.
(23) Maltempo, M. M.; Eaton, S. S.; Eaton, G. R. In *EPR Imaging and in Vivo EPR*; Eaton, G. R., Eaton, S. S., Ohno, K., Eds.; CRC Press: Boca Raton, FL, 1991; Chapter 14, p 145.
(24) *Biological Magnetic Resonance*; Berliner, L. J., Reuben, J., Eds.; Plenum Press: New York, 1989; Vol. 8.
(25) Budil, D. E.; Lee, S.; Saxena, S.; Freed, J. H. *J. Magn. Reson. A* **1996**, *120*, 155.
(26) Pilar, J.; Sikora, A.; Labsky, J.; Schlick, S. *Macromolecules* **1993**, *26*, 137.
(27) Muller, G.; Stadler, R.; Schlick, S. *Macromolecules* **1994**, *27*, 1555−1561.
(28) Kutsumizu, S.; Hara, H.; Schlick, S. *Macromolecules* **1997**, *30*, 2320−2328.
(29) A study of neat ABS based on ESR spectra of various nitroxide spin probes is in support of this statement; see: Varghese, B.; Schlick, S., to be published.
(30) The appearance temperature of the dynamically averaged F spectral component may also depend on the size and motional mechanism of the nitroxide radicals. A larger probe often has an averaged spectral component of type F at a higher temperature compared to a small probe. However, the ESR spectra of the small probe 2,2,6,6-tetramethylpiperidin-1-yloxyl (TEMPO) in neat ABS also indicate that the low-T_g phase in ABS contains not only butadiene but also styrene and/or acrylonitrile; see: Bokria, J.; Schlick, S., to be published.
(31) Carter, R. O., III; McCallum, J. B. *Polym. Deg. Stab.* **1994**, *45*, 1.
(32) Alonso-Amigo, M. G.; Schlick, S. *Macromolecules* **1987**, *20*, 795.
(33) Clough, R. L.; Gillen, K. T. *J. Polym. Sci., Part A: Polym. Chem.* **1989**, *27*, 2313.
(34) Clough, R. L.; Gillen, K. T. *Polym. Deg. Stab.* **1992**, *38*, 47.
(35) Celina, M.; Wise, J.; Ottesen, D. K.; Gillen, K. T.; Clough, R. L. *Polym. Deg. Stab.* **1998**, *60*, 493.
(36) Lucarini, M.; Pedulli, G. F. *Angew. Makromol. Chem.* **1997**, *252*, 179.
(37) Rabello, M. S.; White, J. R. *Polym. Deg. Stab.* **1997**, *56*, 55.
(38) Rabello, M. S. *Plast., Rubber Compos. Process. Appl.* **1998**, *27*, 124.
(39) Jouan, X.; Gardette, J. L. *J. Polym. Sci., Part A: Polym. Chem.* **1991**, *29*, 685.
(40) Jouan, X.; Gardette, J. L. *Polym. Deg. Stab.* **1992**, *36*, 91.
(41) Malik, J.; Hrivik, A.; Tuan, D. Q. In *Polymer Durability: Degradation, Stabilization and Lifetime Prediction*; Clough, R. G., Billingham, N. C., Gillen, K. T., Eds.; Adv. Chem. Ser. 249; American Chemical Society: Washington, DC, 1996; Chapter 29, p 455.

MA001719U